Experimental analysis of heterogeneous nucleation in undercooled melts by infrared thermography

by M. Duquesne*, A. Godin*, E. Palomo del Barrio* and J. Daranlot**

* Univ Bordeaux, I2M, CNRS, UMR 5295, F-33400 Talence, France. CNRS, I2M, UMR 5295, F-33400 Talence, France. Arts et Metiers ParisTech, I2M, UMR 5295, F-33400 Talence, France.

** SOLVAY, Laboratoire du Futur, 178 Av du Dr Schweitzer, 33608 Pessac, France

Abstract

A new experimental technique for quantitative analysis of heterogeneous nucleation in undercooled melts is proposed in this paper. It is based on the observation by infrared thermography of the thermal behavior on cooling of a large population of small droplets deposited on a substrate. The method allows analyzing the influence of different parameters such as the size of the droplets, the cooling rate and the wettability of the substrate on the nucleation rate. The fundamentals of the method, the associated experimental set-up, and the mathematics required for data processing are described in the paper. The results of the nucleation analyses carried out using erythritol deposited on different substrates are also presented and discussed.

Key words: Heterogeneous nucleation, infrared thermography, Singular Value Decomposition.

1. Introduction

Nucleation is the first step of the crystallization of undercooled melts. Homogeneous nucleation is induced in the bulk liquid in the absence of solid surfaces. It is an intrinsic process which exclusively depends on the thermodynamic properties of the studied melt whereas heterogeneous nucleation is an extrinsic process influenced by foreign phases like container walls or impurities. In both cases, nucleation is a random process and can be described by either probability laws or nucleation rates.

Different experimental methods have been developed to study homogeneous nucleation. Most widely used are electromagnetic, electrostatic or acoustic levitation [1,2], short and long Drop-Tube processing [3-5], SAXS/WAXS/DSC techniques [6], and Differential Scanning Calorimeter (DSC) using emulsions [7].

Most of the experimental work dealing with heterogeneous nucleation has been carried out on phase change films deposited on flat substrates. The analysis is performed by direct observation of crystal size and number as a function of time in an isothermal experiment. In-situ transmission electron microscopy (TEM) studies have been performed to accomplish this task [8,9], but the drawbacks of this method are imprecise temperature control and that the electron beam can influence the crystallization due to localized sample heating. To avoid these difficulties, ex-situ atomic force microscope (AFM) in combination with DSC has been proposed [10,11]. Several AFM scanning and annealing cycles are alternatively performed, with the annealing temperature being the same in subsequent anneals. Comparing number density and sizes of crystals on subsequent AFM scans at the same sample location allows estimating the heterogeneous nucleation rate.

This paper proposes an alternative method for studying heterogeneous nucleation. It consists in observing by infrared thermography the thermal behavior on cooling of a large population of small droplets deposited on a flat substrate. The method allows analyzing the influence of different parameters such as the size of the droplets, the cooling rate and the wettability of the substrate on the nucleation rate.

The paper is organized as follows. The classical theory of homogeneous and heterogeneous nucleation is briefly recalled in Section 2. The experimental technique we are proposing for studying heterogeneous nucleation is described in Section 3. The mathematical tools required for raw data processing are presented in Section 4. The results of the nucleation analyses carried out using erythritol deposited on different substrates are presented and discussed in the last section.

2. Recall on the classical theory of nucleation

In the liquid phase, atoms or molecules approach each other statistically, forming crystalline clusters by thermodynamic fluctuations. The thermodynamics of clusters formation was established by Gibbs in 1878. The equilibrium cluster distribution is given by:

$$N(r) = N_o \exp\left(-\frac{\Delta G_{cluster}(r)}{k_B T}\right) \quad (1)$$

*Corresponding Author: marie.duquesne@u-bordeaux.fr

where $\Delta G_{cluster}(r)$ is the reversible work for crystal cluster formation, k_B is the Boltzmann constant, T is the absolute temperature, N_o is the total number of atoms in the liquid per unit volume and $N(r)$ is the number of clusters of radius r at equilibrium. The reversible work for crystal cluster formation can be described as the sum of two contributions:

$$\Delta G_{cluster}(r) = -\frac{4}{3}\pi\, r^3 \Delta G_{lc} + 4\pi\, r^2 \sigma \tag{2}$$

ΔG_{lc} is the free energy difference between the parent and the crystalline phase and $\sigma > 0$ is the interfacial free energy. It can be easily demonstrated that $\Delta G_{cluster}(r)$ passes through a maximum at $r = r_c = 2\sigma / \Delta G_{lc}$. A cluster with radius r_c is called a critical cluster and $\Delta G_c(T) \equiv \Delta G_{cluster}(r_c)$ the critical work for cluster formation. Clusters with $r < r_c$ are energetically not favorable and spontaneously decay, whereas clusters with $r > r_c$ can grow. Therefore, ΔG_c can be considered as an activation barrier against crystallization. The existence of this barrier enables undercooling of a liquid below the melting point T_m without immediate crystallization.

Based on the work of Gibbs, kinetic models for nucleation have been proposed and progressively improved by Volmer and Weber in 1926, Becker and Döring in 1935 and Turnbull and Fisher in 1949. Today, the classical theory is collectively known as the classical theory of nucleation by Volmer, Weber, Becker, Döring, Turnbull and Fisher and it is described in many reference books [12,13]. The steady state nucleation rate ($m^{-3}.s^{-1}$) for homogeneous nucleation can be written as:

$$I^{\hom}(T) = s_c k N_o \Gamma_z \exp\left(-\frac{\Delta G_c(T)}{k_B T}\right) \tag{3}$$

where s_c is the number of surface atoms in the critical cluster, k (s^{-1}) is the arrival rate of parent phase atoms to the critical crystalline cluster, and Γ_z is the Zeldovich factor, which only has a weak temperature dependence. The kinetic pre-factor is equal to $k = 6D/\lambda^2$ for diffusion-limited crystallization, whereas it is equal to $k = u_{sound}/\lambda^2$ for collision-limited crystallization. D is the diffusion coefficient in the liquid or amorphous phase, λ is the average interatomic distance and u_{sound} is the sound velocity in the liquid or amorphous phase.

The classical theory for homogeneous nucleation can equally be applied to the case of heterogeneous nucleation. The only difference is the lower work for critical cluster formation and the reduced number of parent phase atoms that can act as nucleation site. The steady state nucleation rate for heterogeneous nucleation can be written as:

$$\frac{I^{het}(T)}{I^{\hom}(T)} = \varepsilon \exp\left(-\frac{\Delta G_c(T)}{k_B T} f(\theta)\right) \tag{4}$$

$\varepsilon << 1$ is the fraction of parent phase atoms in contact with the heterogeneity and $0 \le f(\theta) \le 1$ is a function of the wetting angle. For crystalline clusters growing on a flat substrate like a spherical cap, $f(\theta) = 0.25(2+\cos\theta)(1-\cos\theta)^2$. Usually, heterogeneous nucleation rates are observed to be far higher (many orders of magnitude) than homogeneous nucleation rates, which implies that θ must be small.

Under non-isothermal conditions (cooling rate $dT/dt \neq 0$) the cumulative distribution function for nucleation is given by:

$$F(T) = 1 - \exp\left[-\frac{v}{dT/dt}\int_{T_m}^{T} I^{\hom/het}(T)\,dT\right] \qquad (0 \le F(T) \le 1) \tag{5}$$

where v represents the volume of the sample. $F(T)$ is a decreasing function of T, with $F(T_m) = 0$. The probability of nucleation is given by $P(T) = dF(T)/dT$.

3. Experimental set-up and procedures

The proposed method is based on the observation by infrared thermography of the thermal behavior on cooling of a large population of small droplets deposited on a flat substrate whose temperature is controlled and known at any time. When a droplet crystallizes, the energy delivered (latent heat) raises the temperature of the droplet/crystal and the signals recorded by the infrared camera at the pixels associated to the droplet show a peak. For small enough droplets, the temperature of crystallization of the droplet can be assumed to be equal to that of the substrate at the time the peak

appears. Once the temperature of crystallization of each droplet has been determined, the probability of nucleation of the product can be easily determined.

3.1 Sample preparation

The preparation of a sample involves melting the product to be analyzed and depositing small droplets of the product on the substrate. The substrate is a thin plate (typically less than 2 mm thickness) made of the chosen material for the heterogeneous nucleation investigation. The droplets deposition on the substrate is done automatically using a robot (Gilson 215 Liquid Handler) provided with a syringe. The robot allows controlling both the size of the droplets (6-25 µl) and their position. As shown in Figure 1, the final population of droplets shows a very narrow size distribution and a quite homogeneous spacing. All the droplets and the substrate is referred as the sample in the following.

In order to warrant that the temperature of the droplet is almost uniform and close to that of the substrate, the use of droplets less than 20 µl is recommended. Besides, a droplets spacing of 9 mm is chosen to avoid that the heat release during the crystallization of one droplet increases the temperature of the neighbor droplets. As plates used are 7.5 cm x 11 cm, the number of droplets by plate is 96. Therefore, several samples have to be tested separately in order to reach a statistically significant number of droplets.

3.2 Experimental setup

Main elements of the experimental setup are the infrared camera (FLIR SC7000, detection window: 1.5-5 µm) and a heating/cooling device (Fig. 1). The highest spatial resolution provided by the infrared camera is about 20 µm. Digital full frame rate of the camera ranges from 170 Hz to 380 Hz, and up to 11 kHz-32 kHz with windowing. The heating/cooling device is a layered structure including:

- A cooling element (bottom layer) which is kept at constant temperature during the experiments and which acts as a heat sink.
- A flat heating resistance which is used to control the thermal course of the sample during the experiments.
- A thermal diffuser (top layer) on which the sample is placed and which is provided with a K-type thermocouple for temperature control.

The setup is mounted on a vibration free solid support and it is provided with a protection box to reduce environment perturbations. A K-type thermocouple for measuring the temperature of the sample is placed on the sample substrate.
The experimental setup allows working temperatures ranging from 3°C to 200°C. The maximum achievable cooling rate is 10°C/min.

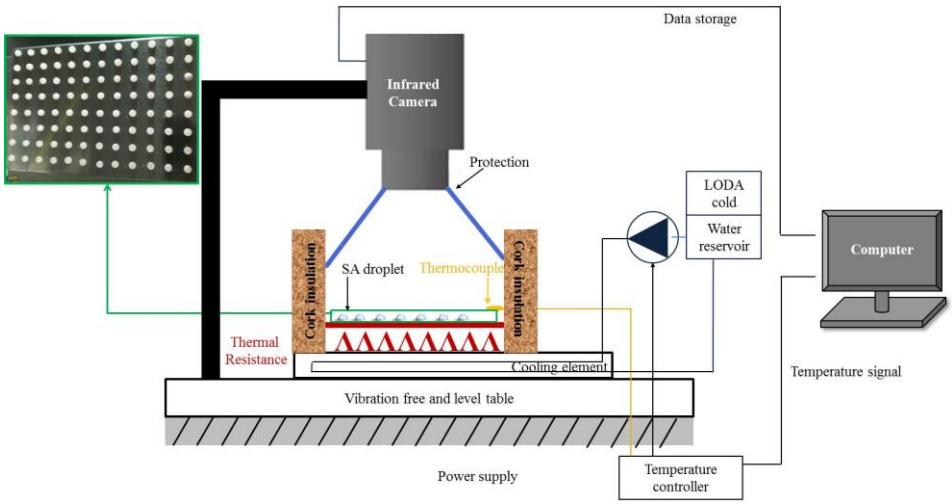

Fig. 1. *Sketch of the experimental device and picture of a sample (framed in green).*

3.2 Testing and raw data

The sample is introduced in the experimental device and is heated above the melting point of the product so that the small crystals become liquid anew. Afterward, the sample is cooled down at a constant cooling rate and its thermal behavior is observed by the infrared camera. Thermal images (205 x 308 pixels) of the sample are recorded at 27 Hz. Simultaneously, the temperature of the substrate is measured by a thermocouple.

As already mentioned, when a droplet crystallizes its temperature is raised and the signals recorded by the infrared camera at the pixels associated to the droplet show a peak (IR-peak hereafter). We remind that the infrared camera doesn't provide direct measurements of temperature, but electrical signals (*DL* = Digital Level) which are proportional to the photonic flux received by the infrared sensors. However, assuming that the temperature of the droplet before crystallization is equal to that of the substrate, the temperature at which the droplet crystallizes can be considered to be equal to the temperature of the substrate at the time the IR-peak appears. Consequently, determining the

crystallization temperature of the droplets in the sample involves identifying the time/substrate temperature at which the IR-peak appears within each droplet.

Figure 2 provides a typical example of results. It represents the spatially averaged values of the DL signals associated to each droplet (one curve by droplet) versus the time (left side) and versus the temperature of the substrate (right side).

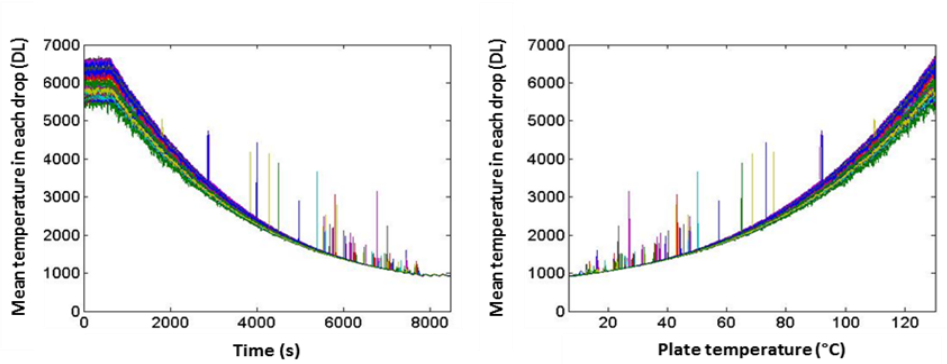

Fig. 2. *Average DL-signals versus time (left side) and versus the plate's temperature (right side).*

4. Data processing

Data recorded during the experiments encompasses thousands of infrared images (205 x 308 pixels) as well as the temperature data of the plate. The steps and the mathematical tools we are proposing for data processing are briefly presented in this section. They aim at automatically and unambiguously identify the time and the temperature at which each droplet crystallizes and at calculating the probability of nucleation as a function of the undercooling.

4.1 Images segmentation

The first step consists in identifying the pixels of the IR-images corresponding to each individual droplet and extracting the DL-signals associated to them. Let $\mathbf{DL}$ be the hyper-matrix $[n_{px} \times n_{py} \times n_t]$ containing the whole set IR-images, where $n_{px} \times n_{py}$ is the number of pixels by image (205 x 308 pixels) and n_t the total number of images. The whole set of infrared images are reduced to one-single image by averaging $\mathbf{DL}$ on time. The average IR-image captures main information regarding the position of the droplets on the plate and is segmented by thresholding to produce a new binary image in which all pixels unambiguously associated to the droplets are identified by a single value (1) and the rest of the pixels (background) are all 0-valued. The connected components of the foreground of the binary image are then split in a set of disjoined elementary objects (individual droplets). This in done using the general procedure outlined in reference [14]. Once elementary objects have been conveniently labelled, the DL-signals associated to each droplet can be easily retrieved. Figure 3 displays the grayscale average IR-image of one of the experiments carried out (left side), the corresponding binary image (center). Pixels unambiguously associated to a droplet are in red, while all other pixels are in blue. In the last image (Fig. 3, right), each droplet on the plate is identified by a different arbitrary color.

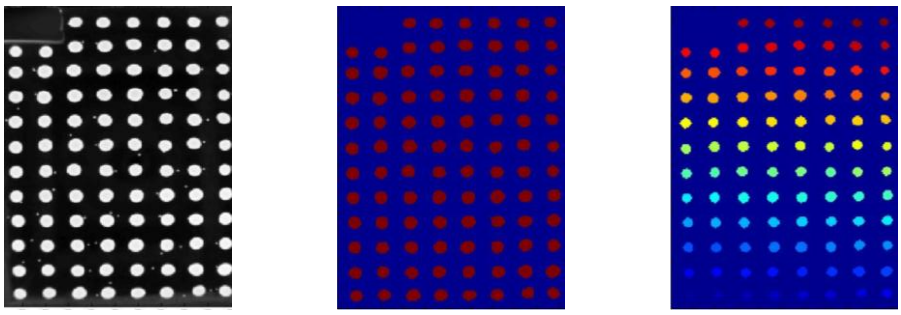

Fig. 3. *Example of a grayscale average IR images (left), the corresponding binary image (center) and the image including disjoined droplets in arbitrary colors (right).*

4.2 Signals analysis and determination of the probability of nucleation

In the second step, a droplet-by-droplet analysis is carried out to identify the temperature at which each droplet crystallizes. Let $\mathbf{X}$ be the matrix $[n_p \times n_t]$ containing the DL-signals corresponding to one-single droplet, where n_p is the number of pixels associated to the droplet and n_t the total number of time samples. As shown in Figure 4, the peak

of crystallization in the DL-signals can be significant (left side) and easy to detect automatically by simple differentiation of the signals, but it can also be very small (center and right side). In the latter case, the time series differentiation usually fails in the peak detection because of the measurement noise. To automatically identify the peaks of crystallization, even when they are very small, DL-signals are hence submitted to several transformations.

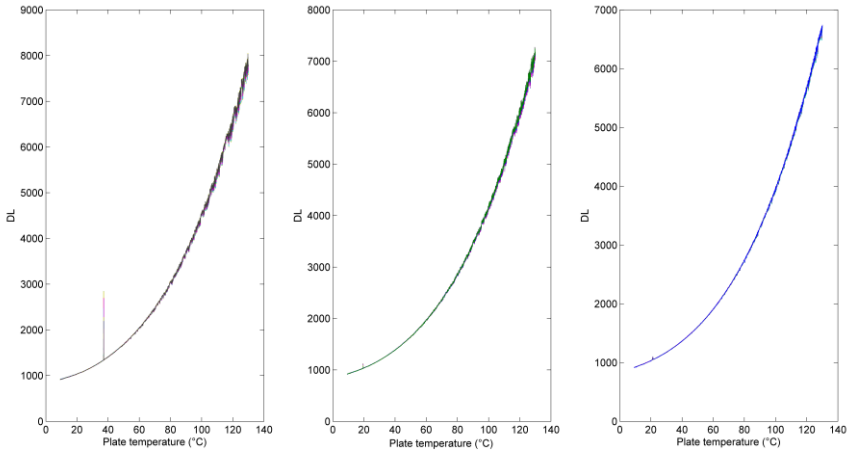

Fig. 4. *Examples of DL-signals vs. the plate temperature.*

The first transformation is defined by

$$\mathbf{X} \leftarrow \mathbf{X}^{0.25} \tag{6}$$

It aims at reducing the non-linearity in the functional relationship existing between the DL-signals and the plate temperature. As shown in Figure 5, this transformation also leads to an amplification of the crystallization peak. However, the peak can still be small compared to measurement noise.

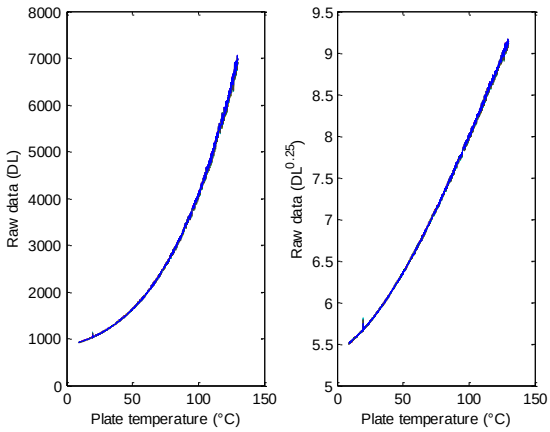

Fig. 5. *Example of DL-signals (left) and $DL^{1/4}$- signals versus the plate temperature.*

To overcome this difficulty, a singular value decomposition (SVD) is applied to the $DL^{0,25}$ data. SVD is a well known technique that is widely used in image processing and signal processing problems for compression and noise reduction purposes [15, 16]. The SVD of $\mathbf{X}$ can be written as:

$$\mathbf{X} = \mathbf{C}\mathbf{Z}(t) \tag{7}$$

$\mathbf{C}$ $[n_p \times n_p]$ is a constant matrix that includes the eigenvectors of the covariance matrix of the data, whereas $\mathbf{Z}(t) = [Z_1(t), Z_2(t), \cdots, Z_{n_p}(t)]'$ $[n_p \times n_t]$ is a time-dependent matrix that contains the coefficients which results of projecting $\mathbf{X}$ on $\mathbf{C}$. Figure 6 shows the time evolution of the coefficients $Z_1(t), Z_2(t), Z_3(t), Z_4(t)$ derived from the singular value decomposition of the data in Figure 5. The first coefficient of projection reproduces the appearance of the initial signal. Therefore, it does not bring any new information about the peak of crystallization. However, the peak of crystallization is significantly amplified in the other three coefficients of projection.

To facilitate the automatic recognition of the peak of crystallization just by looking at the maximum and minimum Z-values, the trend in the signals Z_2 to Z_4 is then eliminated:

$$Z_i(t) \leftarrow Z_i(t) - m_i(t) \tag{8}$$

$m_i(t)$ represents the trend in $Z_i(t)$ $(i = 2,3,4)$ and it is calculated by applying a smoothing procedure of "moving average" type to these signals. The obtained results for Z-signals in Figure 6 are shown in Figure 7.

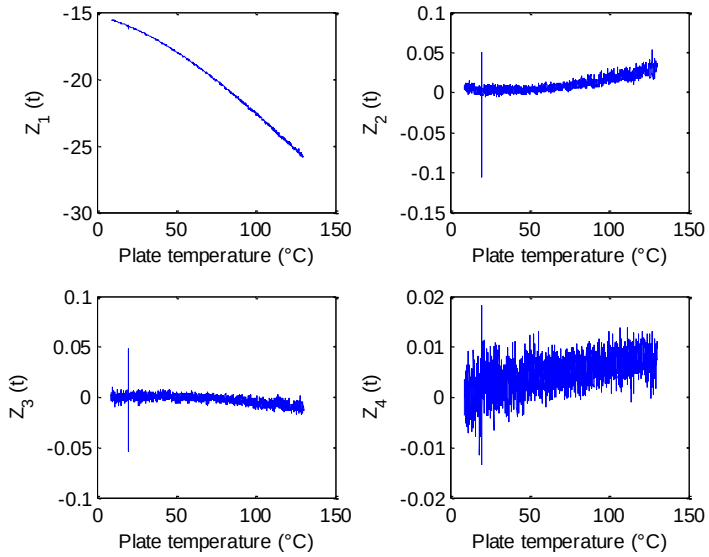

Fig. 6: *Time evolution of first four coefficients of projection.*

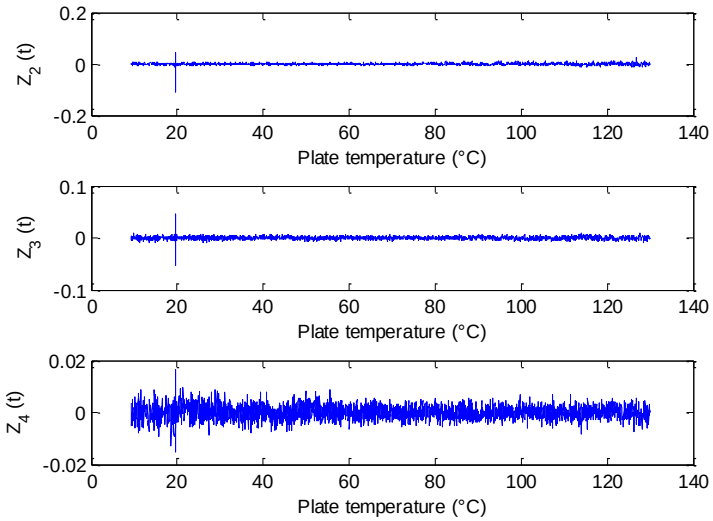

Fig. 7. *Evolution of the coefficients of projection Z_2, Z_3 et Z_4 over time after de-trending.*

The temperature at which the analyzed droplet crystallizes can then be easily determined:

1. First, the maximum and the minimum values ($Z_{i,max}$, $Z_{i,min}$) of $Z_i(t)$ (i=2,3,4) are calculated and compared to the standard deviation σ_i of $Z_i(t)$. Only extreme values ($Z_{i,max}$, $Z_{i,min}$) verifying $abs(Z_{i,max}/\sigma_i) > k$ and $abs(Z_{i,min}/\sigma_i) > k$ (k = threshold) are considered to be significant peaks and potentially related to the droplet crystallization.
2. For significant peaks, the plate temperature at the time the peak appear is determined (peak's temperatures). The temperature at which the droplet crystallizes is considered to be equal to the mean value of the non-aberrant peak's temperatures.

The analysis is carried out on $Z_i(t)$ (i=2,3,4) simultaneously because the peak of crystallization is not always significant in the three series, from one side, and it could be significant in e.g. $Z_i(t)$ (i=3,4) but not in $Z_2(t)$, from another side.

Once the temperature of crystallization of each droplet has been determined, the cumulative distribution function associated to the nucleation process is estimated as:

$$F(T) = n(T)/N \tag{9}$$

where $n(T)$ is the number of droplets that have been already crystallize at temperature $T \leq T_m$, T_m is the melting point of the product and N is the total number of droplets that are tested. The probability of nucleation is the derivative of cumulative distribution function with respect to temperature: $P(T) = dF(T)/dT$.

5. Experimental results

The method proposed for heterogeneous nucleation analysis has been applied to determine the probability of nucleation of erythritol in contact with different substrates.

5.1. Materials: Erythritol and the substrates

Erythritol ($C_4H_{10}O_4$) is a sugar alcohol usually used as sugar replacer [17] and more recently as phase change material for thermal energy storage purposes [18-20]. The melting point and the latent heat of erythritol are, respectively, 118°C and 340 (J/g) [21].

Four different substrates have been considered: "Aluminium 800", "Aluminium 1200", "Stainless steel" and "Brass 800". Both, "Aluminium 800" and "Aluminium 1200" are made of aluminium but their surfaces have been polished with different sizes of grit sandpaper (800 and 1200). "Stainless steel" is made of commercial polished stainless steel and "Brass 800" is made of brass polished with 800 grit sandpaper. The plates used in the tests are of dimensions 11 cm x 7,5 cm and 2 mm of thickness.

The roughness of the plates surface has been measured with an HOMMELTESTER T500 roughnessmeter. The plate is placed on a heating element and roughness measurements are performed at temperatures ranging from 20°C to 65°C. To investigate the uniformity of the surfaces and to calculate uncertainties, the plates are divided in nine sections (Fig. 8) and the measurements are carried out independently on each section. The roughness of a surface is evaluated through two statistical parameters: the average amplitude of the roughness (Rz), and the arithmetical mean of the distances (in absolute value) between the actual surface and the mean surface (Ra). In the range of the tested temperatures, no significant changes of roughness with temperature have been observed. Parameters Rz and Ra obtained are reported in Table 2.

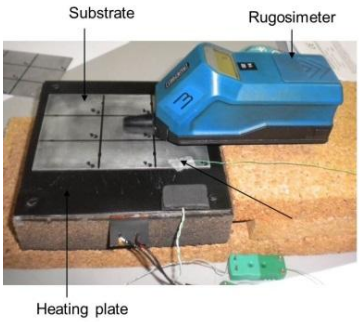

Fig. 8. *Experimental set up using the roughnessmeter.*

	Ra (µm)	Rz (µm)
Brass 800	0,135 ± 0,065	1,213 ± 0,527
Stainless steel	0,173 ± 0,0330	1,664 ± 0,836
Aluminium 1200	0,439 ± 0,099	3,568 ± 0,772
Aluminium 800	0,667 ± 0,173	5,198 ± 0,978

Table 2. *Roughness measurements from 20°C to 65°C.*

The wettability of the substrates has been analyzed by direct measurement of the wetting angle θ. The used experimental set up is sketched in Figure 10. The substrate is placed on a heating element in order to control the temperature. A droplet of erythritol (10 mg) is then carefully deposited on the substrate and a picture is taken with a high resolution optical camera (Genie HM1024). As shown in Figure 10, a back-light is used to increase the contrast between the droplet and the background. The picture of the droplet is then processed as indicated in Figure 9 (left side) to determine the contact angle. The droplets are small enough to neglect the gravity effect on the form of the droplet. Indeed, the droplets form a perfect spherical cap in all the cases (see Fig. 9, left).

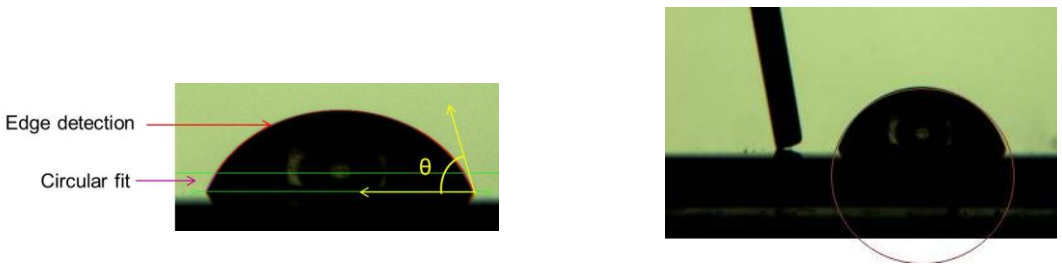

Fig. 9. *Images of a droplet of erythritol on the "Aluminium 800" substrate at 90°C: Contact angle determination (left side) and verification of the spherical form of the droplet (Scale: a syringe tip of 700-µm thickness is placed near the droplet).*

Besides, the Bond number has been calculated and it is always less than 0.455.

$$Bo = \frac{\rho g R^2}{2\sigma_{LG}}(1-\cos\theta) \tag{10}$$

ρ is the density of erythritol (ρ = 1300 kg.m^{-3}), g is the gravity (g = 9.81 m.s^{-2}), R is the radius of the droplet, θ is the contact angle and σ_{LG} is the surface tension at the interface between the melt and the air (σ_{LG} = 28 mN.m^{-1}).

The measurements are carried out at different positions on the substrate in order to take into account structural and/or chemical heterogeneities of the surface as well as roughness variability. All the tests have been performed at 90°C. The results obtained are reported in Table 3. As shown in Figure 11, there is a strong correlation between roughness and wettability. Whatever may be the nature of the substrate (brass, aluminium, steel), the contact angle decreases with the roughness of the surface.

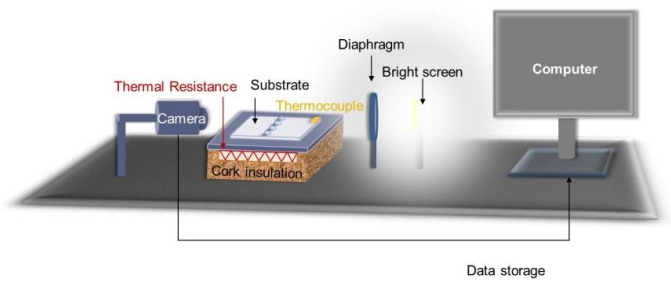

Fig.10. *Setup for contact angle measurements.*

	Number of droplets	Average contact angle θ (°)
Brass 800	76	60,06 ± 1,8627
Stainless steel	70	54,206 ± 1,844
Aluminium 1200	45	50,0867 ± 1,7994
Aluminium 800	82	47,1695 ± 1,8366

Table 3. *Contact angle measurements.*

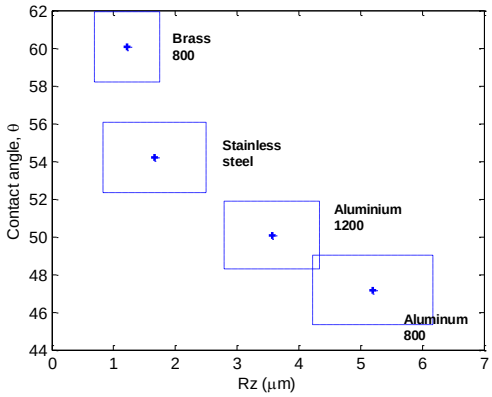

Fig. 11*. Contact angle vs. roughness: mean values (cross) and uncertainties (square).*

5.3. Tests carried out and results

The tested samples are described in Tables 5 and 6. Those in Table 5 have been used to study the influence of the size of the droplets on the probability of nucleation whereas those in Table 6 allows analyzing the influence of the substrate. In all the cases, the sample is first heated up to 130°C (10°C above the melting point) and stabilized at this temperature during 10 min. Afterwards, the sample is cooled down from 130°C to 10°C at 1°C/min. At last, a second isothermal at 10°C during 10 minutes is applied.

The cumulative distribution function for the nucleation process F(T) (shortly nucleation distribution function) has been determined as explained in Section 4. By definition, F(T) is 0 at the melting point T=T_m and takes values between 0 and 1 for T<T_m. Besides, the probability of nucleation is given by P(T)=dF(T)/dT. Figure 12 (left side) represents the nucleation distribution function for erythritol droplets on the "Aluminium 800" substrate. The blue line corresponds to droplets of 6.8 mg whereas the red line is the result obtained with droplets of 16.5 mg. In both cases, four different regimes of nucleation can be distinguished: 1) a first regime in which the probability of nucleation is very low, with F(T) values less than 0.05; 2) a second regime in which the probability of nucleation increases progressively; 3) a third regime with maximum values of probability of nucleation (maximum slope of F(T)); and 4) a last regime in which F(T) becomes equal to 1 (all the droplets are crystallized). As expected, the first regime is shortened when increasing the size of the droplets. Indeed, 5% of the droplets of 16.5 mg are crystallized at T= 80°C whereas the temperature has to be T=50°C for 5% of the droplets of 6.8 mg crystallize. Besides, for any value of T, the values of the nucleation distribution function are higher for droplets of 16.5 mg than for the other droplets (6.8 mg).

	Number of droplets	Weight of droplets
Aluminium 800	680	6,8 ± 0.6 mg
Aluminium 800	546	16,5 ± 1 mg

Table 5. *Test carried out with two sizes of the droplets deposited on the same aluminium 800.*

	Brass 800	Stainless steel	Aluminium 1200	Aluminium 800
Number of droplets	624	558	564	564
Weight of droplets	10,5 ± 1 mg	10,5 ± 1 mg	10,5 ± 1 mg	10,5 ± 1 mg

Table 6. *Test carried out 10 mg-droplets deposited on different plates polished with two types of grit sandpaper.*

Figure 12 (right side) represents the nucleation distribution function of erythritol droplets of 10.5 mg deposited on the "Brass 800" (blue line), "Stainless steel" (red line), "Aluminium 1200" (black line), and "Aluminium 800" (green line). As previously, all these curves show four different regimes of nucleation. It can be observed that the probability of nucleation is very low in the temperature range from 50°C to 120°C in all the cases. The nucleation distribution function is similar for the three substrates with higher wettability (contact angles between 47-54°), namely "Stainless steel", "Aluminium 1200", and "Aluminium 800". However, the nucleation distribution function is always below for the substrate showing the highest contact angle (Brass 800, θ =60°) when T<50°C. As predicted theoretically, the nucleation rate increases when the contact angle decreases and the probability of nucleation is hence higher for "Stainless steel", "Aluminium 1200", and "Aluminium 800".

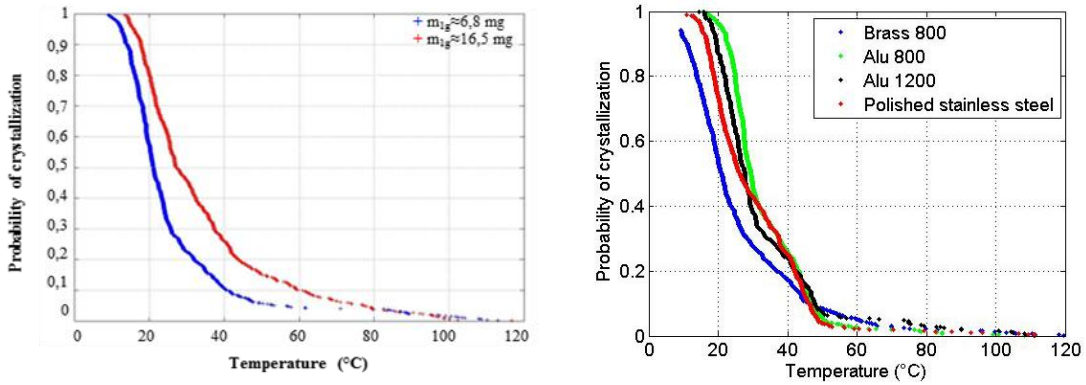

Fig. 12. *Nucleation distribution functions. Left side: for droplets of 6,8 mg (blue curve) and 16,5 mg (red curve) deposited on "Aluminium 800"; Right side: for 10mg-droplets deposited on plates made of aluminium 800 (green curve) and 1200 (black curve), commercial polished stainless steel (red curve), and brass 800 (blue curve).*

6. Conclusion

A new experimental technique for quantitative analysis of heterogeneous nucleation in undercooled melts has been proposed. It is based on the observation by infrared thermography of the thermal behavior on cooling of a large population of small droplets deposited on a flat substrate. Specific infrared images and data processing has been proposed to identify the temperature at which each droplet crystallize. The method has been applied to determine the probability of nucleation of erythritol in contact with different substrates. The influence of different parameters such as the size of the droplets and the wettability of the substrate have been studied. The results achieved seems to be in agreement with theory. However, other tests will be required to complete the validation of the proposed method and to define the limits.

Acknowledgment

The authors acknowledge the financial support of the European Commission for subsidizing SAM.SSA (Sugar Alcohols based Materials for Seasonal Storage Applications) Project within the 7th framework program for research. We also want to thank the SARO Company (http://www.saro-usinage.fr/contact.html) for helping to determine the surfaces roughness.

REFERENCES

[1] Wu Y., Piccone T. J., Shiohara Y., Flemings M. C., "Dendritic growth of undercooled Nickel-Tin: Part 1", Metallurgical Transactions A., 18(6), 915-924, 1987.

[2] Herlach D.M., Cochrane R.F., Egry I., Fecht H.J., Greer A.L., Containerless processing in the study of metallic melts and their solidification, International Materials Review,38(6),273-347,1993.

[3] T.J. Rathz, M.B. Robinson, W.H. Hofmeister and R.J. Bayuzick, The Marshall Space Flight Center Drop Tube Facility, Review of Scientific Instruments, 61, 3846, 1990.

[4] Vinet B., Cortella L., Favier J. J. and Desre P., Highly undercooled W and Re drops in an ultrahigh-vacuum drop tube, Applied Physics Letters, 58, 97,1991.

[5] Drehman A.J., Turnbull D., "Solidification behavior of undercooled Pd83Si17 and Pd82Si18 liquid droplets", Scripta Metallurgica, 15, 543-548, 1981.
[6] Ryan A.J, Fairclough A., Terrill N.J, Olmsted P.D., Poon W.C.K, "A scattering study of nucleation phenomena in polymer crystallization", Faraday Discussions, 112, pp.13-29, 1999.
[7] Dumas J.P., Zeraouli Y., Strub M., "Heat transfer inside emulsions. Determination of the DSC thermograms Part 1. Crystallization of the undercooled droplets", Thermochimica Acta, vol. 236, pp. 227-237, 1994.
[8] Privitera S., Bongiorno C., Rimini E., Zonca R., "Crystal nucleation and growth processes in $Ge_2Sb_2Te_5$", Applied Physics Letters, 84 (22), 4448-4450, 2004.
[9] G. Ruitenberg, A. K. Petford-Long and R. C. Doole, Determination of the isothermal nucleation and growth parameters for the crystallization of thin Ge2Sb2Te5 films, Journal of Applied Physics, 92, 3116, 2002.
[10] Kalb J. A., Wen C. Y., Spaepen F., Dieker H., Wuttig M., Crystal morphology and nucleation in thin films of amorphous Te alloys used for phase change recording, Journal of Applied Physics, 98, 054902, 2005.
[11] Kooi B.J., Groot W.M.G., De Hosson J.Th.M., *In situ* transmission electron microscopy study of the crystallization of Ge2Sb2Te5, Journal of Applied Physics, 95, 924-932, 2004.
[12] Fredriksson H., Akerlind U, "Solidification and Crystallization Processing in metals and Alloys", John Wiley & sons, ISBN: 978-1-119-99305-6.
[13] Herlach D., Galenko P., Holland-Moritz D., "Metastable Solids from Undercooled Melts", Pergamon Materials Series Elsevier, 2007.
[14] Haralick R. M., Shapiro L.G., "Computer and Robot Vision, Volume 1", Addison-Wesley, 28-48, 1992.
[15] Deprettere F., "SVD and signal processing: algorithms, analysis and applications", Elsevier Science Publishers, Amsterdam, 1988.
[16] B.S. Everitt, and G. Dunn, "Applied multivariate data analysis", Arnold, London, 2001.
[17] Livesey G., "Health potential of polyols as sugar replacers, with emphasis on low glycaemic properties", Nutrition Research Reviews, 16, pp. 163-191, 2003.
[18] Lee S-Y., Park M., Park S-J., "Thermal characterization of erythritol/expanded composites for high thermal storage capacity, Carbon, 68, 67-72, 2014.
[19] Oya T., Nomura T., Tsubota M., Okinaka N., Akiyama T., "Thermal conductivity enhancement of erythritol as PCM by using graphite and nickel particles", Applied Thermal Engineering, 61, 825-828, 2013.
[20] Wang W., He S., Guo S., Yan J., Ding J., "A combined experimental and simulation study on charging process of Erythritol–HTO direct-blending based energy storage ", Energy Conversion and Management, 83, 306-313, 2014.
[21] E. Palomo del Barrio, "Formulation and screening", 2nd Progress Meeting, FP7 project -SAM.SSA-Work package 3, Valencia, March 2013.